Effect of Spin-Orbit Coupling on Decay Widths of Electronic Decay Processes

Elke Fasshauer[a*]

[a]*Department of Physics and Astronomy, Aarhus University, Ny Munkegade 120, 8000 Aarhus, Denmark*

(Dated: May 19, 2020)

Abstract

Auger-Meitner processes are electronic decay processes of energetically low-lying vacancies. In these processes, the vacancy is filled by an electron of an energetically higher lying orbital, while another electron is simulataneously emitted to the continuum. In low-lying orbitals relativistic effects can not even be neglected for light elements. At the same time lifetime calculations are computationally expensive. In this context, we investigate which effect spin-orbit coupling has on Auger-Meitner decay widths and aim for a rule of thumb for the relative decay widths of initial states split by spin-orbit coupling. We base this rule of thumb on Auger-Meitner decay widths of Sr4p^{-1} and Ra6p^{-1} obtained by relativistic FanoADC-Stieltjes calculations and validate it against Auger-Meitner decay widths from the literature.

*Email:Elke.Fasshauer@gmail.com

I. INTRODUCTION

Electronic decay processes are initiated by a sub-outer valence ionization or excitation. The system relaxes by filling the vacancy with an electron and transferring the excess energy to another electron of the system, which is emitted. One examples of electronic decay processes is the well known Auger process. It was first discovered by Lise Auger-Meitner [1] and later rediscovered by Pierre Auger [2]. In order to give credit where credit is due and following the renaming suggestion of Ref. [3] we will refer to it as the Auger-Meitner process. It is found in a variety of different systems like atoms, molecules and solids. As a consequence, Auger-Meitner spectroscopy is used for surface analysis in metallurgy, quality analysis of microelectronics as well as for basic studies of chemical reaction mechanisms [4]. Since the advent of short XUV pulses, it has been a test process for time-resolved measurements [5, 6] and is often observed as a side product of modern x-ray spectroscopies [7]. Another relevant and interesting process is the family of Interparticle Coulombic Decay processes (ICD) [8–10]. A deeper understanding of the effects that determine the decay widths of electronic decay processes, that can lead to rule of thumbs, which do not require expensive lifetime calculations will be helpful for the interpretation of the observed spectra. This article aims to provide such a rule of thumb for relative Auger-Meitner decay widths of initial states split by spin-orbit coupling. In the following, we will assume processes initiated by ionization.

In order to occur, two criteria need to be fulfilled: the energy and the coupling criterion. To fulfill the energy criterion the final state energy is required to be lower than the energy of the singly ionized initial state. If this is not the case, the channel defined by a certain doubly ionized final state is closed and the corresponding fragments of the channel are not observed after the decay. To fulfill the coupling criterion, the decay process needs to be fast enough to prevail over other energetically accessible decay pathways like radiative relaxation or coupling to nuclear degrees of freedom. It hence contains the information whether an energetically allowed process can be expected to be observed experimentally or not. Therefore, a typical study of electronic decay processes consists of two parts:

- determination of the kinetic energy of the secondary electron and, as a consequence, which decay channels are open

- calculation of the decay width $\Gamma = \frac{\hbar}{\tau}$, which is proportional to the decay rate $\frac{1}{\tau}$ and inversely proportional to the lifetime τ

The primary ionization often removes an electron from an atomic core, where relativistic effects are stronger than for valence electrons. The relativistic effects can therefore be expected to play a crucial role for the understanding of the systems' lifetimes. Phenomenologically, the relativistic effects can be divided into spin-orbit coupling and scalar-relativistic effects. The spin-orbit coupling requires the system to be described in terms of the total angular momentum j rather than the orbital momentum l and the spin momentum s. Thereby the non-relativistically degenerate states of one particular l value are split into two states with $j = l \pm s$ of different energies [11]. The scalar-relativistic effects result in spatial contractions of all orbitals on one-electron systems. In many-electron systems, however, those orbitals with density close to the nucleus are more strongly contracted than others. They thereby shield the positive charge of the nucleus from the electrons in other orbitals, which are therefore effectively spatially decontrated compared to the non-relativistic solutions. Therefore, as a rule of thumb, s and p are spatially contracted while d and f orbitals are spatially decontrated. [11].

The initial and final state energies can be obtained using a variety of quantum chemical approaches.

One is known in the literature as the Algebraic Diagrammatic Construction [12–17] (ADC), which is also available for a fully relativistic treatment [18–20]. The calculation of the respective lifetimes is a challenging task, because it requires the description of both bound and continuum electrons. The bound electrons are best described by wavefunctions with $\mathcal{L}^2$ boundary conditions, while continuum electrons far away from the atom are best described by plane waves. This imposes the technical choice between a) describing the entire atom using an $\mathcal{L}^2$ basis, b) describing the entire process using a grid, or c) describing the bound electrons using an $\mathcal{L}^2$ basis and the continuum electron using a grid. Either of these approaches faces difficulties in either describing the bound or the continuum states or some artificially constructed interface region. Traditionally, most quantum chemical program packages are based on $\mathcal{L}^2$ bases and we therefore choose to describe the electronic decay processes using a large $\mathcal{L}^2$ basis for convenience.

The quantum chemical methods, which have been developed for a relativistic description of the decay widths are the Multichannel Multi-Configurational Dirac-Fock (MMCDF) [21]

and the FanoADC-Stieltjes [22, 23]. The MMCDF is limited to atomic systems and strongly depends on the manual selection of CI (Configuration Interaction) components to be included in the description of initial and final states. The FanoADC-Stieltjes is based on the ADC and not limited to spherically symmetric systems. It is furthermore size-consistent and includes terms up to third order in perturbation theory yielding the interaction between initial and final state without actually calculating the states themselves. It is therefore a good compromise between accuracy and computational cost. At the same time, the configurations needed for the accurate description of initial and final states are determined automatically up to the implemented order of the perturbed wavefunction. The FanoADC-Stieltjes approach is implemented in the relativistic quantum chemistry package DIRAC [24], which allows to use different Hamiltonians while keeping all other parameters constant. This allows us to computationally only consider scalarrelativistic effects using Dyall's spinfree Hamiltonian [25] as well as performing a fully relativistic calculation using the four-component Dirac-Coulomb (DC) Hamiltonian taking both scalarrelativistic and spin-orbit coupling into account. By comparing the results, we can extract the effect caused by spin-orbit coupling. We therefore choose the FanoADC-Stieltjes approach for our calculations.

In this work we focus on the atomic Auger-Meitner process in order to exploit basic knowledge about the influence of relativistic effects, but we expect the conclusions to hold for molecular Auger-Meitner process and Interparticle Coulombic Decay (ICD) processes [8–10, 26] as well. The Auger-Meitner decay process initiated by a photoionization can most generally be described by:

$$A \quad \xrightarrow{h\nu} \quad (A^+)^* + e^-_{\mathrm{ph}} \quad \xrightarrow{\text{Auger-Meitner}} \quad A^{2+} + e^-_{\mathrm{ph}} + e^-_{\mathrm{sec}}$$

A system A is ionized, while the photo-electron e^-_{ph} is emitted. Afterwards, the actual Auger-Meitner process of the initial state A^+ can occur. An electron from an outer shell fills the vacancy and the excess energy is instantaneously transferred to another (secondary) electron e^-_{sec}, which is subsequently emitted. The final state of the decay process is to be described by a doubly charged atom A^{2+} and the secondary electron in the continuum. In the special case when the vacancy filling electron or the secondary electron stem from an orbital of the same shell as the initial vacancy the process is called Coster-Kronig decay. When both are from the same shell, the process is referred to as super-Coster-Kronig decay. These Coster-Kronig decays are characterized by very large decay widths. [27] We will

discuss these special cases separately from the Auger Meitner process in this paper.

We have previously shown, how scalar-relativistic effects influence the decay widths of the Auger-Meitner process in noble gas atoms. [23] After primary ionization from the $(n-1)d$ orbitals the noble gas atoms decay to np^{-2}, $np^{-1}ns^{-1}$ and ns^{-2} final states. We observed that the Auger-Meitner decay widths increased by up to 326 % for radon by including scalar-relativistic effects in the calculation. This dramatic increase could be explained by the larger spatial overlap of the orbitals involved in the decay compared to non-relativistic calculations due to a contraction of the s and p orbitals of the final states.
However, the fully relativistic calculation resulted in different decay widths for the different $d_{3/2}^{-1}$ and $d_{5/2}^{-1}$ initial states split by spin-orbit coupling (see Fig. 5 of Ref. [23]). The aim of this work is therefore to investigate the influence of spin-orbit coupling on the decay widths of electronic decay processes. For this purpose, we will study the Auger-Meitner processes of earth alkaline atoms after primary ionization from the $(n-1)p$ orbitals. The earth alkaline elements have the benefit of a single and closed shell ns^{-2} final state. This might allow us to purely observe how the spin-orbit splitting of the different initial states affects the Auger-Meitner decay width. Moreover, in the single particle picture, a Coster-Kronig decay is possible for neither of the initial states of the earth alkaline elements and thus the pure Auger-Meitner process, where the initial states have an equal number of possible decay channels, can be observed. Having only one final state, which is not affected by spin-orbit coupling, reduces the complexity of the analysis of the results significantly.

The paper is structured as follows: in section II we recapitulate the basics of the FanoADC-Stieltjes method. We then give the computational details for our ab initio calculations in section III. We present the results and their interpretation in section IV and conclude in section V.

II. THEORY

Following Wentzel [28] and later Feshbach [29, 30] and Fano [31] the decay width of a decay process initiated by a primary ionization is given by

$$\Gamma = \sum_{\beta} 2\pi \left| \langle \Phi | \hat{V} | \chi_{\beta,\varepsilon} \rangle \right|^2 . \tag{1}$$

Here, $|\Phi\rangle$ and $|\chi_{\beta,\varepsilon}\rangle$ denote the initial and final state, respectively. $\hat{V}$ is the interaction operator of the initial and final states, which in Feshbach's definition is known as H_{PQ}. The index β refers to the different decay channels and ε denotes the energy of the final state. Eq. (1) thereby connects the metastable initial and the continuum final states. They are constructed by partitioning the Hamiltonian into two subspaces. The initial (final) state is then an eigenfunction of this initial (final) state sub-space Hamiltonian. However, finding proper solutions to both the initial and the final states on an equal footing is a non-trivial task, because they adhere to different boundary conditions. Since the final state depends on the energy of the emitted electron, any approach needs to either determine the continuum state or to mimic the final state using $\mathcal{L}^2$-functions. While the continuum functions are normalized with respect to their energy

$$\langle \chi_\varepsilon | \chi_{\varepsilon'} \rangle = \delta(\varepsilon - \varepsilon') \tag{2}$$

the $\mathcal{L}^2$ approach is based on a discrete set of final states $|\tilde{\chi}_{\tilde{E}}\rangle$ which adhere to different boundary conditions and are normalized with respect to space (see e.g. [32])

$$\langle \tilde{\chi}_{\tilde{E}_i} | \tilde{\chi}_{\tilde{E}_j} \rangle = \delta_{ij}. \tag{3}$$

Because of this different normalization the decay widths are not amenable to a direct calculation. As first proposed by Hazi [33], for autoionization processes such difficulties can be solved by using the Stieltjes-Chebyshev moment theory also called Stieltjes imaging [34–36]. It relies on the observation that the moments of order k of the projected final state Hamiltonian H_f

$$\mu_k = \langle \Phi | \hat{V} H_f^k \hat{V} | \Phi \rangle \tag{4}$$

calculated from the determined discrete pseudo-spectrum are good approximations to the moments determined from the real continuum states. This can be shown by inserting the resolution of identity for the continuum states

$$\mu_k = \sum_i \varepsilon_i^k \left| \langle \Phi | \hat{V} | \chi_{i,\varepsilon} \rangle \right|^2 + \int_{E_0}^{\infty} \varepsilon^k \left| \langle \Phi | \hat{V} | \chi_\varepsilon \rangle \right|^2 \mathrm{d}\varepsilon. \tag{5}$$

Since the non-zero contribution to the coupling matrix elements in the Feshbach-Fano approach stems only from an interaction region of finite size, where the $\mathcal{L}^2$ final state func-

tions are nonvanishing, we may replace the expansion $\sum_i |\chi_{i,\varepsilon}\rangle \langle\chi_{i,\varepsilon}| + \int \mathrm{d}\varepsilon\, |\chi_\varepsilon\rangle \langle\chi_\varepsilon|$ by its $\mathcal{L}^2$ approximation $\sum_j |\tilde{\chi}_{\tilde{E}_j}\rangle \langle\tilde{\chi}_{\tilde{E}_j}|$ (see [37])

$$\mu_k \approx \sum_j \tilde{E}_j^k \left|\langle\Phi|\hat{V}|\tilde{\chi}_{\tilde{E}_j}\rangle\right|^2. \tag{6}$$

Then the decay width can be determined through a series of consecutive approximations to the moments of increasing order k.

To achieve this kind of description, we choose the relativistic FanoADC-Stieltjes approach. Here, a proper selection of $2h1p$ intermediate state configurations are used for the description of the continuum final state, while the rest is used for the description of the initial state. The resulting discrete pseudo-spectrum is then subject to a Stieltjes imaging procedure. An exhaustive description of the method can be found in Refs. [23] and [38].

III. COMPUTATIONAL DETAILS

The Auger-Meitner decay widths were calculated with the relativistic FanoADC-Stieltjes method implemented in the relativistic quantum chemical program DIRAC [24]. We included up to third order contributions of perturbation theory and additional constant diagrams. For each element four-component calculations based on the Dirac-Coulomb (DC) Hamiltonian and scalarrelativistic spinfree calculations were performed for both the $(n-1)p_{1/2}$ and $(n-1)p_{3/2}$ initial states. Dyall's cv4z basis sets [39] were augmented with additional diffuse 5s5p5d3f basis functions following the Kaufmann-Baumeister-Jungen approach [40]. The resulting moments were checked for numerical instabilities. Only those moments, without numerical instabilities entered the interpolation scheme for the determination of the decay widths as described in Ref. [23].
The radial orbital densities of the ions were calculated using GRASP [41, 42].

IV. RESULTS

In order to analyze the decay processes, we first discuss the energetic accessibility of different decay channels and then present the corresponding Auger-Meitner decay widths. In Fig. 1 we present the computed single and double ionization spectra of strontium obtained by DC-ADC calculations. The main peaks of the ionization from the $\mathrm{Sr}4p_{3/2}$ and the

Sr$4p_{1/2}$ have single ionization potentials (SIPs) of 28.277 eV and 29.402 eV, respectively. The experimental values of 28.21 eV and 29.17 eV are very close and verify the applicability of the chosen method [43]. They are characterized by pole-strengths, which in this implementation is defined as the sum of the absolute squares of the $1h$ coefficients [44], of 0.76 and 0.80 (see Table II). We will at this point treat them as single configurations and analyze them in detail later. These two single ionization energies are higher than only one double ionization potential (DIP) of 16.430 eV, which is to 99.7 % characterized by the double ionization from the $5s$ valence. The Auger-Meitner process is therefore energetically accessible and results in a single final state. For radium the spectra are qualitatively the same and lead to the same conclusion.

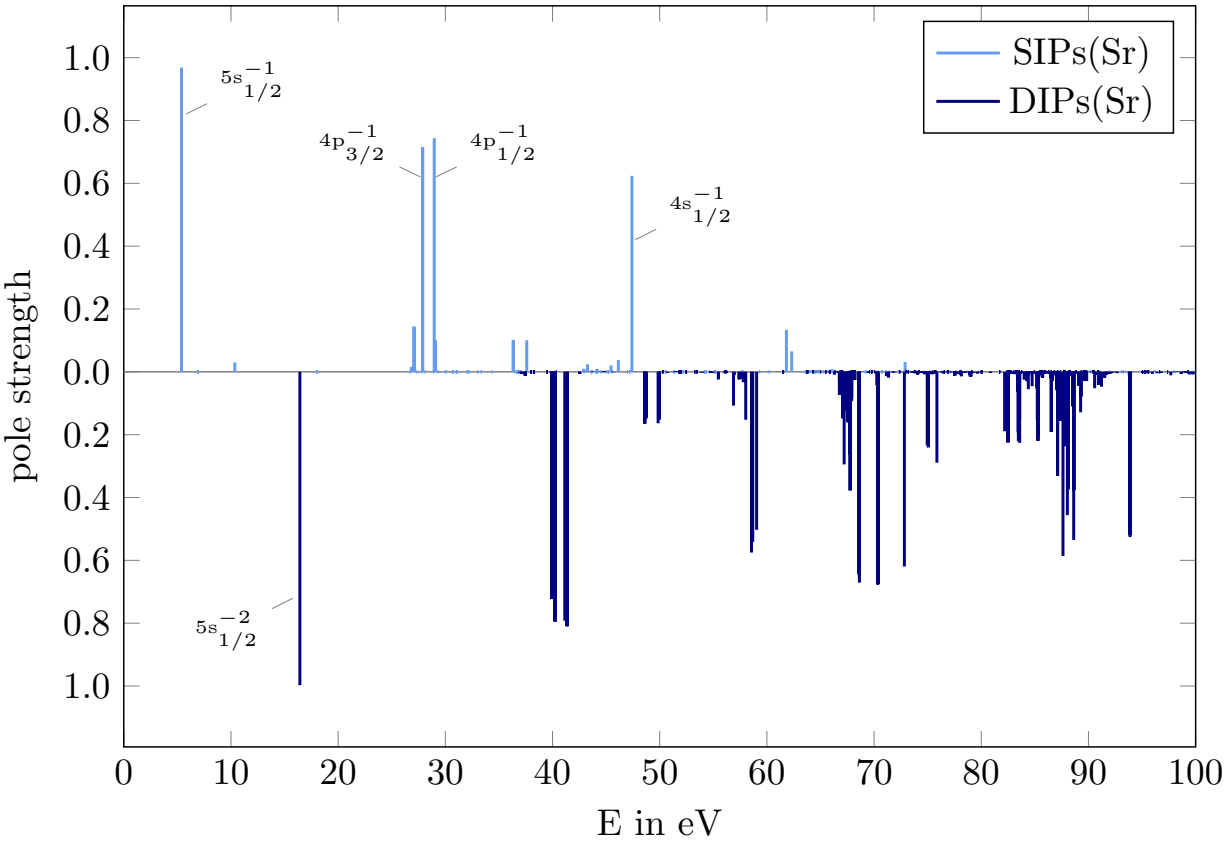

Figure 1: Comparison of the single (SIP) and double (DIP) ionization spectra of the strontium obtained by a DC-ADC calculation.

We show the corresponding decay widths of strontium and radium obtained by relativistic FanoADC-Stieltjes calculations in Table II for the scalarrelativistic spinfree $(n-1)p^{-1}$ as well as the fully relativistic $(n-1)p^{-1}_{1/2,1/2}$, $(n-1)p^{-1}_{3/2,1/2}$ and $(n-1)p^{-1}_{3/2,3/2}$ initial states.

Table I: Ionization energies, pole-strengths P and decay widths Γ of different Auger-Meitner initial states of strontium and radium obtained by relativistic FanoADC-Stieltjes calculations.

initial state	energy [eV]	P	Γ[meV]
Sr spinfree	28.599	0.78	0.56
Sr4$p_{1/2,1/2}$	29.402	0.80	0.10
Sr4$p_{3/2,1/2}$	28.277	0.76	1.23
Sr4$p_{3/2,3/2}$	28.277	0.76	1.17
Ra spinfree	21.836	0.49	28.56
Ra6$p_{1/2,1/2}$	25.494	0.78	0.26
Ra6$p_{3/2,1/2}$	19.267	0.50	93.16
Ra6$p_{3/2,3/2}$	19.267	0.50	98.86

They are illustrated in Fig. 2. To the best of my knowledge, the Auger-Meitner decay widths of these systems have not been presented in the literature so far.

Despite the difference in absolute numbers, the decay widths of the different initial states show the same pattern. The decay width of the $(n-1)p^{-1}_{1/2,1/2}$ initial state is lowest, while the decay widths of the $(n-1)p^{-1}_{3/2,1/2}$ and $(n-1)p^{-1}_{3/2,3/2}$ initial states are close and significantly higher than for the $(n-1)p^{-1}_{1/2,1/2}$ initial state. As the atomic $(n-1)p^{-1}_{3/2,1/2}$ and $(n-1)p^{-1}_{3/2,3/2}$ states are degenerate, their complex energies, i.e., the decay widths should also be equal. It may be possible to estimate the error of the calculations from the observed deviation. However, this concept needs to be proven for a larger set of data points. In case of the strontium atom, the decay width of the $p_{3/2}$ initial state is approximately 12 times larger than the decay with of the $p_{1/2}$ initial state. In radium, the corresponding factor is 380. Furthermore, the decay width average of the $p_{3/2}$ initial state is increased by 114 % and 236 % for strontium and radium, respectively. We can therefore observe an increase of the decay width difference of the $p_{3/2}$ initial state both compared to the $p_{1/2}$ and spinfree initial state for heavier atoms. How can this result be understood?

Considering our previous findings about the role of scalarrelativistic effects on electronic decay widths [23], we inspect the radial densities of the $(n-1)p$ and the ns orbitals of the strontium and radium ions, which we assume to be involved in the decay process (see Fig. 3). In case of the strontium atom, the radial densities of the $4p_{1/2}$ and the $4p_{3/2}$ orbitals

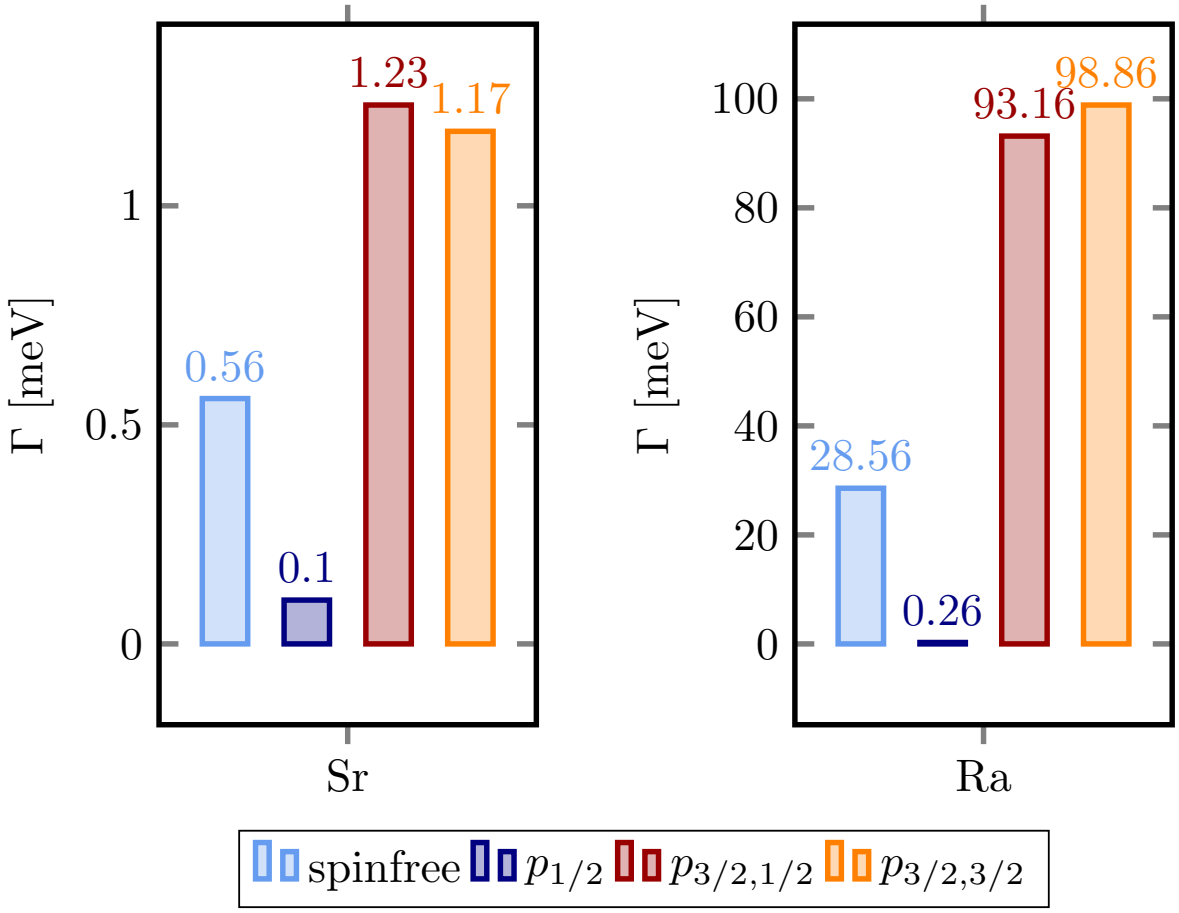

Figure 2: Decay widths of strontium and radium after primary ionization from an $(n-1)p$ orbital obtained by relativistic FanoADC-Stieltjes calculations with different Hamiltonians. The spinfree Hamiltonian includes only scalarrelativistic effects, while the four-component DC Hamiltonian also includes spin-orbit coupling, which gives rise to three possible initial states: the $p_{1/2}^{-1}$ as well as the degenerate $p_{3/2,1/2}$ and $p_{3/2,3/2}$ initial state. The decay width of the $p_{1/2}$ initial state is significantly lower than for either of the $p_{3/2}$ initial states.

are almost identical. But for the radium atom, the radial density of the $6p_{1/2}$ orbital is closer to the nucleus than the radial density of the $6p_{3/2}$ orbital. This general property of a stronger contraction of the $l-1/2$ than the $l+1/2$ orbital is already visible in the analytic solutions of the one-electron system [45, 46] and the corresponding radial expectation values $\langle r \rangle$. The differences of the radial expectation values increases with the nuclear charge Z. In many electron systems, where the contraction of the wavefunction decreases with the total angular momentum j, this effect is enlarged. Because the Auger-Meitner decay rates

crucially depend on the overlap of the involved orbitals, the decay widths of an $(n-1)p_{3/2}^{-1}$ initial state can be expected to be higher than the decay widths of an $(n-1)p_{1/2}^{-1}$ initial state. These findings are reflected in the decay widths shown in Fig. 2 and Table II and are consistent with the observations of the noble gas Auger-Meitner processes in Ref. [23].

Table II: Radial expectation values $\langle r \rangle$ of orbitals involved in the Auger-Meitner process for different configurations given in Ångström.

$\langle r \rangle$	config.	$(n-1)p_{1/2}$	$(n-1)p_{3/2}$	$(n-1)d_{3/2}$	$(n-1)d_{5/2}$	$ns_{1/2}$
Sr	$4p^5 5s^2$	0.794	0.809	–	–	1.981
	$4p^5 4d5s$	0.802	0.818	1.332	1.375	2.062
Ra	$6p^5 7s^2$	0.996	1.114	–	–	2.244
	$6p^5 6d7s$	1.001	1.120	1.768	1.821	2.290

However, the simulations of Auger-Meitner processes in other earthalkaline elements have shown that correlation effects are important for the correct description of these elements' decay widths. Both the investigations of the Auger-Meitner process following primary ionization from the $2p$ orbitals of calcium [47] as well as from the $4d$ orbitals of barium [48] showed the necessity to include excitations from the valence s orbital to the d orbitals, which are unpopulated in the ground state, in the description of the initial state. In our case, this would require to include the following configurations in our simulations: $(n-1)p^{-1}\,ns^2$, $(n-1)p^{-1}\,(n-1)d\,ns$ and $(n-1)p^{-1}\,(n-1)d^2$. Thereby, a fast Coster-Kronig decay is enabled equally for both the $l-1/2$ as well as the $l+1/2$ case.

Indeed, the analysis of the ADC eigenvectors of the initial states of both strontium and radium showed that beyond the single and main $1h$ contribution of the respective p orbital, the initial state is mainly characterized by $2h1p$ configurations of the $(n-1)p^{-1}\,ns\,d$ kind. The $(n-1)p^{-1}\,(n-1)d\,ns$ configurations are therefore automatically included in our simulations. The relativistic FanoADC-Stieltjes implementation is, however, limited to second order perturbations in the wavefunction and therefore does not go beyond $2h1p$ configurations. This means that the $(n-1)p^{-1}\,(n-1)d^2$ configurations are not taken into account in this work.

How do these configurations affect the decay widths? Since the overlap of the orbitals involved in the decay determine the decay widths, we show the radial densities of the orbitals

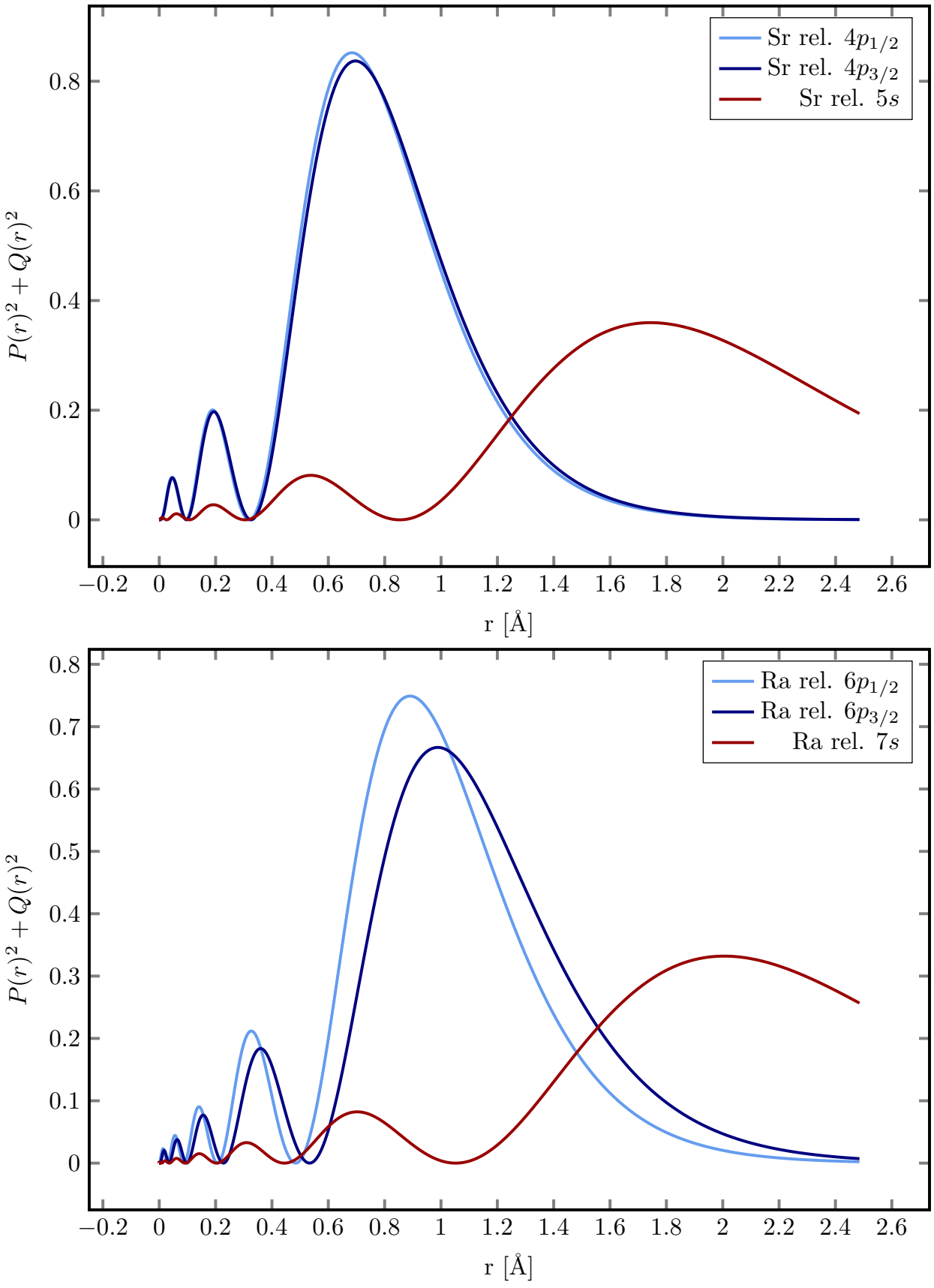

Figure 3: Radial densities of the orbitals of the $(n-1)p^5s^2$ ions involved in the Auger-Meitner decay. The expectation value of the electrons position of the $(n-1)p_{1/2}$ orbital is lower than of the respective $(n-1)p_{3/2}$ orbitals. The ns orbitals of the ions experience a stronger contraction the those of the atom (not shown here).

involved in the decay of the $6p^5 6d7s$ configuration of radium in Fig. 4. The $6p$ orbitals are slightly more contracted than in the $6p^{-1}\,7s^2$ configuration, while the $7s$ orbital is slightly decontracted by a difference of the electron's distance from the nucleus $\Delta\langle r\rangle$ of 0.046 Å. However, the $6d$ orbitals, which are involved in the Auger-Meitner process of this configuration, show a large overlap with both the $6p$ and the $7s$ orbitals. The corresponding decay width should therefore be larger than the decay width of the $6p^{-1}\,7s^2$ configuration. The prevalence of the $(n-1)p_{3/2}$ decay width over the $(n-1)p_{1/2}$ also holds for this configuration. If the $(n-1)p^{-1}\,(n-1)d^2$ configurations have non-negligible contributions, the presented decay widths of Table II would be lower bounds to the results of a more accurate decay width calculation.

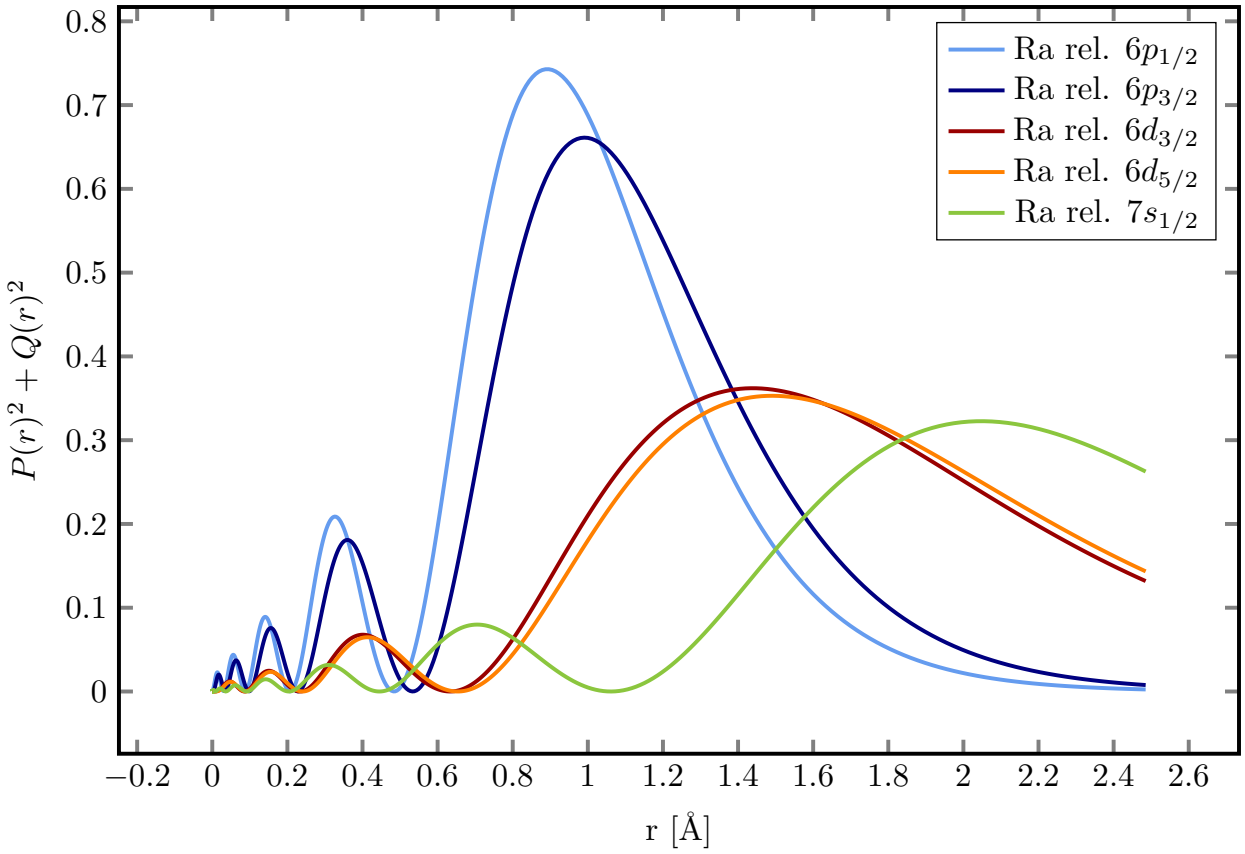

Figure 4: Radial densities of the radium orbitals of the ionic $6p^5 6d7s$ configuration involved in the Auger-Meitner decay. The overlap of the radial densities of the $6p$ orbitals with the radial densities of the $6d$ orbitals is more pronounced than with the radial density of the $7s$ orbital.

The observed differences in the decay widths for different initial states and Hamiltonians can therefore not only be accounted for by relativistic effects, but different contributions

of the $(n-1)p^{-1}\,d\,ns$ configurations may also affect the result. In this case, the required measure of the $(n-1)p^{-1}\,ns^2$ configuration's contribution to the ionized initial state is the pole-strength, which are listed for the different initial states in Table II. The analysis of the eigenvectors, where the different contributions have been classified according to the main hole, $(n-1)p^{-1}\,d\,ns$, which includes the $(n-1)p^{-1}\,(n-1)d\,ns$ configurations, and other, is shown in Table III and illustrated in Figure 5.

Table III: Eigenvector analysis of the decaying initial states.

	Configuration	spinfree	$p_{1/2,1/2}$	$p_{3/2,1/2}$	$p_{3/2,3/2}$
Sr	$(n-1)p^{-1}$	0.782	0.798	0.756	0.756
	$(n-1)p^{-1}\,ns^{-1}d$	0.050	0.089	0.101	0.084
	$(n-1)p^{-1}\,ns^{-1}(n-1)d$	0.000	0.002	0.002	0.002
	other	0.160	0.107	0.140	0.153
Ra	$(n-1)p^{-1}$	0.494	0.777	0.497	0.497
	$(n-1)p^{-1}\,ns^{-1}d$	0.412	0.011	0.395	0.396
	$(n-1)p^{-1}\,ns^{-1}(n-1)d$	0.005	0.000	0.005	0.005
	other	0.086	0.195	0.099	0.086

The significant contributions beyond the main hole is of the $(n-1)p^{-1}\,ns\,d$ kind. We therefore assume that they are the only other contributions and that their contribution is $1-P$. For strontium, the pole-strengths are similar but not identical for all initial states and Hamiltonians. At the same time both the contribution of the $(n-1)p^{-1}\,ns^{-1}(n-1)d$ configuration and the manifold of $(n-1)p^{-1}\,ns^{-1}d$ configurations are similar in all 4-component cases. We can therefore predominantly attribute the decay width difference between the $p_{3/2}$ and $p_{1/2}$ initial state to spin-orbit coupling rather than the differences in the contributions of the $4p^5 4d5s$ configuration. For radium, however, the pole-strengths of the initial states differ. The $6p_{1/2}$ initial state has a pole-strength of 0.78, while both the initial state of the scalarrelativistic Hamiltonian and the $6p_{3/2}$ initial state have much lower pole-strengths of 0.49 and 0.50, respectively. The $6p^{-1}\,7s^2$ configuration is therefore predominant for the $6p_{1/2}$ initial state, while it is not for the $6p_{3/2}$ initial state. We can therefore not attribute the discrepancy of the decay widths of the $6p_{1/2}$ and $6p_{3/2}$ initial states to spin-orbit splitting alone. However, the initial state determined with the spinfree

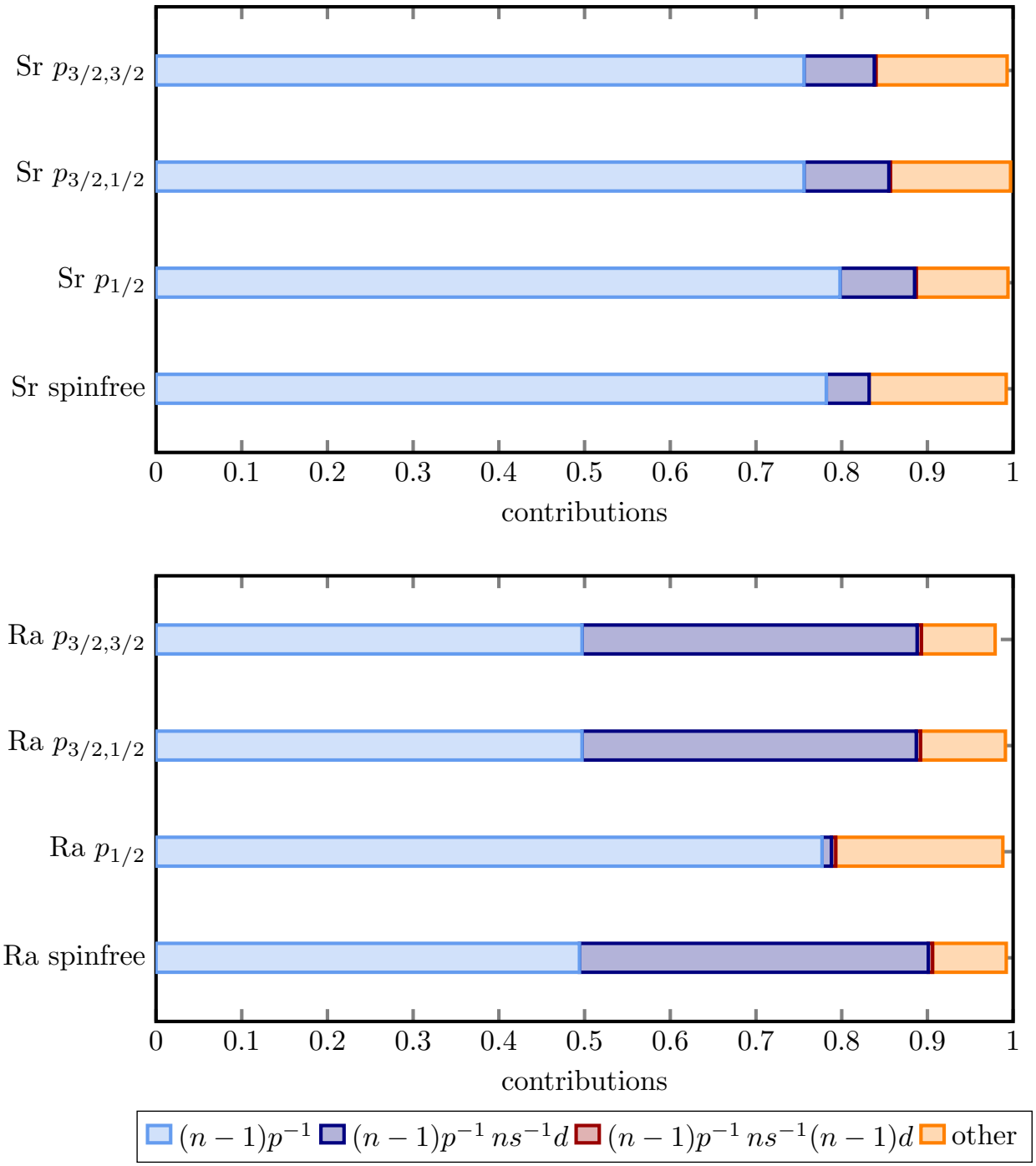

Figure 5: Illustration of the eigenvector analysis of the different initial states listed in Table III. While the pole strength is similar for all Hamiltonians and initial states for strontium, it differs for different initial states in the case of radium. However, the contributions to the spinfree, $p_{3/2,1/2}$ as well as $p_{3/2,3/2}$ initial state are very similar.

Hamiltonian has a pole-strength comparable to the $6p_{3/2}$ initial states as well as equal contribution of the $(n-1)p^{-1}\,ns^{-1}(n-1)d$ configurations and similar contribution of the manifold of $(n-1)p^{-1}\,ns^{-1}d$ configurations but the decay width of the $6p_{3/2}$ initial state is increased by 236 % compared to the spinfree result. Hence, we can explain the increase of the decay width from the spinfree to the $6p_{3/2}$ initial state by spin-orbit coupling.

Based on these consistent findings, we can formulate the following rule of thumb for the relative Auger-Meitner decay widths:
Two ionized initial states that stem from the same non-relativistic configuration and are split by spin-orbit coupling will have different decay widths, where the decay width of the $l-\frac{1}{2}$ initial state will be significantly lower than the decay width of the $l+\frac{1}{2}$ initial state. In contrast to the effect imposed by scalarrelativistic effects, this rule of thumb is independent of the angular moment quantum number l, because the $l-\frac{1}{2}$ will always be contracted more strongly than the corresponding $l+\frac{1}{2}$ orbital and the final state orbitals will be further away from the nucleus than the initial state orbitals. The difference can be expected to increase with the atomic number Z, because the difference of orbital contraction increases with Z.

The question is whether this rule of thumb is applicable to the Auger-Meitner processes of other elements. For this, we refer to the Auger-Meitner and Coster-Kronig decay widths of L and M initial states extracted from Refs. [49–51] and presented in Tables IV – VI. We note that this data is limited to comparably heavy elements as simulations of Auger-Meitner decay widths based on relativistic wavefunctions are unavailable in the literature for lighter elements.

It is readily seen that the formulated rule of thumb holds for the Auger-Meitner for all cases but one. The latter is the Auger-Meitner process of manganese after primary ionization of a $2p$ orbital (see Table IV). However, the rule of thumb is not correct, when Coster-Kronig processes contribute unequally to the decay of the $l+1/2$ and $l-1/2$ initial states. The $L3$ and the $M5$ initial states are unable to undergo a Coster-Kronig decay and they, as well as the $M3$ initial state have one fast decay channel less than their $l-1/2$ counterpart. One may expect an increasing trend for the ratio of the decay widths with the nuclear charge Z. For the L_2 and L_3 as well as the M_4 and M_5 shells only few data points contradict this hypothesis, while no clear trend can be seen for the M_2 and M_3 shells.

Based on the above reasoning, one would also expect this rule of thumb to extend to ICD and Electron Transfer Mediated Decay (ETMD) processes as well. The ICD decay widths

Table IV: Auger-Meitner (AM) decay widths and Coster-Kronig (CK) widths of L_2 and L_3 shells in eV extracted from Ref. [49].

Z	Element	$\Gamma_{\mathrm{AM}}(L_2)$	$\Gamma_{\mathrm{AM+CK}}(L_2)$	$\Gamma_{\mathrm{AM}}(L_3)$
25	Mn	0.390	–	0.337
30	Zn	0.664	–	0.689
36	Kr	1.101	1.219	1.167
40	Zr	1.373	1.578	1.465
45	Rh	1.705	2.029	1.860
47	Ag	1.832	2.192	2.028
50	Sn	2.016	2.454	2.256
52	Te	2.128	2.614	2.406
54	Xe	2.236	2.767	2.557
56	Ba	2.336	2.912	2.696
60	Nd	2.456	3.060	2.897
63	Eu	2.534	3.146	3.041
67	Ho	2.611	3.233	3.211
70	Yb	2.662	3.285	3.340
74	W	2.753	3.423	3.543
80	Hg	2.877	3.600	3.878
90	Th	3.060	3.877	4.464
92	U	3.082	4.272	4.571
96	Cm	3.126	5.386	4.805
98	Cf	3.146	5.360	4.934
100	Fm	3.168	5.586	5.060

partly depend on the transition dipole moment between the initial and final state of the initially ionized unit, which in return increases with the overlap of the electron densities of the involved orbitals. The ETMD decay widths are determind by the orbital overlap of two different units, which is larger for orbitals further away from the nucleus. Hence the same argumentation as for the Auger-Meitner process should be possible in both cases. A

Table V: Auger-Meitner (AM) decay widths and Coster-Kronig (CK) widths of M_2 and M_3 shells in eV extracted from Ref. [50].

Z	Element	$\Gamma_{\mathrm{AM}}(M_2)$	$\Gamma_{\mathrm{AM+CK}}(M_2)$	$\Gamma_{\mathrm{AM}}(M_3)$	$\Gamma_{\mathrm{AM+CK}}(M_3)$
67	Ho	0.687	9.484	0.977	9.823
70	Yb	0.277	10.259	1.125	9.949
74	W	0.839	11.870	1.342	10.529
78	Pt	1.257	13.148	1.569	9.735
80	Hg	1.313	13.580	1.673	10.166
85	At	1.403	13.597	1.990	10.879
88	Ra	1.634	14.169	2.170	10.667
90	Th	1.650	14.404	2.264	9.973
92	U	1.727	14.557	2.375	10.235
95	Am	1.836	15.130	2.629	10.850

Table VI: Auger-Meitner (AM) decay widths and Coster-Kronig (CK) widths of M_4 and M_5 shells in eV extracted from Ref. [51].

Z	Element	$\Gamma_{\mathrm{AM}}(M_4)$	$\Gamma_{\mathrm{AM+CK}}(M_4)$	$\Gamma_{\mathrm{AM}}(M_5)$
70	Yb	1.408	2.445	1.460
74	W	1.758	1.831	1.830
80	Hg	2.259	2.381	2.452
83	Bi	2.512	2.670	2.753
88	Ra	2.923	3.126	3.253
92	U	3.203	3.528	3.611
96	Cm	3.646	4.089	4.075
100	Fm	4.000	4.488	4.583

validation will be left for future work.

V. CONCLUSIONS

We have presented lower bounds for decay widths for the Auger-Meitner process initiated by ionization from the $(n-1)p$ orbitals of strontium and radium. Through analysis of results from different Hamiltonians and initial state eigenvectors as well as radial densities of orbitals involved in the Auger-Meitner process, we were able to show the importance of configuration interaction in this specific case and the effect of spin-orbit coupling on decay widths of electronic decay processes in general. We condensed our findings into the following rule of thumb for the decay widths of electronic decay processes: Two ionized initial states that stem from the same non-relativistic configuration and are split by spin-orbit coupling will have different decay widths, where the decay width of the $l - \frac{1}{2}$ initial state will be significantly lower than the decay width of the $l + \frac{1}{2}$ initial state. We have tested this rule of thumb against Auger-Meitner decay widths available in the literature and could thereby validate it for the majority of cases.

VI. ACKNOWLEDGEMENTS

The author would like to thank the audience of the REHE 2017 conference for raising the main question addresed in this article and acknowledges funding from the Villum foundation.

VII. DATA AVAILABILITY STATEMENT

The data that support the findings of this study are available from the corresponding author upon reasonable request.

[1] L. Meitner, Z. Phys. **9**, 131 (1922).

[2] P. Auger, C. R. Acad. Sci. **177**, 169 (1923).

[3] D. Matsakis, A. Coster, B. Laster, and R. Sime, Phys. Today **72**, 10 (2019).

[4] M. P. Seah, "Microscopic methods in metals," (Springer, Berlin, Heidelberg, 1986) Chap. Auger Electron Spectroscopy.

[5] M. Drescher, M. Hentschel, R. Kienberger, M. Uiberacker, V. Yakovlev, A. Scrinzi, T. Westerwalbesloh, U. Kleineberg, U. Heinzmann, and F. Krausz, Nature **419**, 803 (2002).

[6] O. Smirnova, V. S. Yakovlev, and A. Scrinzi, Phys. Rev. Lett. **91**, 253001 (2003).

[7] G. Greczynski and L. Hultman, Mat. Sci. **107**, 100591 (2020).

[8] L. S. Cederbaum, J. Zobeley, and F. Tarantelli, Phys. Rev. Lett. **79**, 4778 (1997).

[9] U. Hergenhahn, J. Electron Spectrosc. Relat. Phenom. **184**, 78 (2011).

[10] T. Jahnke, J. Phys. B: Atomic, Molecular and Optical Physics **48**, 082001 (2015).

[11] M. Reiher and A. Wolf, *Relativistic Quantum Chemistry* (Wiley-VCH Verlag GmbH, 2009).

[12] J. Schirmer, *Many-Body Methods for Atoms, Molecules and Clusters*, Lecture Notes in Chemistry (Springer Nature Switzerland AG, 2018).

[13] J. Schirmer, Phys. Rev. A **26**, 2395 (1982).

[14] J. Schirmer, L. S. Cederbaum, and O. Walter, Phys. Rev. A **28**, 1237 (1983).

[15] J. Schirmer, Phys. Rev. A **43**, 4647 (1991).

[16] J. Schirmer, A. B. Trofimov, and G. Stelter, J. Chem. Phys. **109**, 4734 (1998).

[17] F. Mertins and J. Schirmer, Phys. Rev. A **53**, 2140 (1996).

[18] M. Pernpointner and A. B. Trofimov, J. Chem. Phys. **120**, 4098 (2004).

[19] M. Pernpointner, J. Chem. Phys. **121**, 8782 (2004).

[20] M. Pernpointner, J. Phys. B **43**, 205102 (2010).

[21] S. Fritzsche, A. N. Grum-Grzhimailo, E. V. Gryzlova, and N. M. Kabachnik, J. Phys. B **44**, 175602 (2011).

[22] V. Averbukh and L. S. Cederbaum, J. Chem. Phys. **123**, 204107 (2005).

[23] E. Fasshauer, P. Kolorenč, and M. Pernpointner, J. Chem. Phys. **142**, 144106 (2015).

[24] DIRAC, a relativistic ab initio electronic structure program, Release DIRAC17 (2017), written by L. Visscher, H. J. Aa. Jensen, R. Bast, and T. Saue, with contributions from V. Bakken,

K. G. Dyall, S. Dubillard, U. Ekström, E. Eliav, T. Enevoldsen, E. Faßhauer, T. Fleig, O. Fossgaard, A. S. P. Gomes, E. D. Hedegård, T. Helgaker, J. Henriksson, M. Iliaš, Ch. R. Jacob, S. Knecht, S. Komorovský, O. Kullie, J. K. Lærdahl, C. V. Larsen, Y. S. Lee, H. S. Nataraj, M. K. Nayak, P. Norman, G. Olejniczak, J. Olsen, J. M. H. Olsen, Y. C. Park, J. K. Pedersen, M. Pernpointner, R. di Remigio, K. Ruud, P. Sałek, B. Schimmelpfennig, A. Shee, J. Sikkema, A. J. Thorvaldsen, J. Thyssen, J. van Stralen, S. Villaume, O. Visser, T. Winther, and S. Yamamoto (see http://www.diracprogram.org).

[25] K. G. Dyall, J. Chem. Phys. **100**, 2118 (1994).

[26] S. Marburger, O. Kugeler, U. Hergenhahn, and T. Möller, Phys. Rev. Lett. **90**, 4 (2003).

[27] D. Coster and R. D. L. Kronig, Physica **2**, 13 (1935).

[28] G. Wentzel, Z. Physik **43**, 524 (1927).

[29] H. Feshbach, Ann. Phys. **5**, 357 (1958).

[30] H. Feshbach, Ann. Phys. **19**, 287 (1962).

[31] U. Fano, Phys. Rev. **124**, 1866 (1961).

[32] J. Craigie, A. Hammad, B. Cooper, and V. Averbukh, J. Chem. Phys. **141**, 014105 (2014).

[33] A. Hazi, J. Phys. B **11**, L259 (1978).

[34] P. W. Langhoff, C. T. Corcoran, F. Sims, J. S. Weinhold, and R. M. Glover, Phys. Rev. A **14**, 1042 (1976).

[35] C. T. Corcoran and P. W. Langhoff, J. Math. Phys. **18**, 651 (1977).

[36] F. Müller-Plathe and G. H. F. Diercksen, in *Electronic Structure of Atoms, Molecules and Solids* (Kluwer Academic Publishers, 1990).

[37] W. P. Reinhardt, Comp. Phys. Comm. **17**, 1 (1979).

[38] E. Fasshauer, *Investigation of Relativistic Effects in Electronic Decay Processes in Small and Large Noble Gas Clusters by Ab Initio and New Simulation Approaches*, `Ph.D.thesis`, University of Heidelberg (2014).

[39] K. G. Dyall, J. Phys. Chem. A **113**, 12638 (2009).

[40] K. Kaufmann, W. Baumeister, and M. Jungen, J. Phys. B **22**, 2223 (1989).

[41] K. G. Dyall, I. P. Grant, F. A. Parpia, and E. P. Plummer, Comp. Phys. Comm. **55**, 425 (1989).

[42] F. A. Parpia, C. Froese Fischer, and I. P. Grant, Comp. Phys. Comm. **94**, 249 (1996).

[43] W. Schmitz, B. Breuckmann, and W. Mehlhorn, J. Phys. B **9**, L493 (1976).

[44] A. B. Trofimov and J. Schirmer, The Journal of Chemical Physics **123**, 144115 (2005).

[45] H. A. Bethe and E. Salpeter, *Quantum mechanics of one- and two-electron atoms* (Plenum Publ. Co., New York, 1977).

[46] V. M. Burke and I. P. Grant, Proceedings of the Physical Society **90**, 297 (1967).

[47] J. Nikkinen, H. Aksela, S. Heinäsmäi, E. Kukk, N. Berrah, and S. Aksela, Phys. Scripta **T115**, 119 (2005).

[48] S. J. Rose, I. P. Grant, and J. P. Connerade, Phys. Trans. Royal Soc. London **296**, 527 (1980).

[49] M. H. Chen, B. Crasemann, and H. Mark, Phys. Rev. A **24**, 177 (1981).

[50] M. H. Chen, B. Crasemann, and H. Mark, Phys. Rev. A **27**, 2989 (1983).

[51] M. H. Chen, B. Crasemann, and H. Mark, Phys. Rev. A **21**, 449 (1980).